Review

Reformulation of Theories of Kinematic Synthesis for Planar Dyads and Triads

Sean Mather * and Arthur Erdman

Department of Mechanical Engineering, University of Minnesota, 111 Church Street SE, Minneapolis, MN 55455, USA
* Correspondence: mathe587@umn.edu

Abstract: Methods for solving planar dyads and triads in kinematic synthesis are scattered throughout the literature. A review of and a new compilation of the complex number synthesis method for planar dyads and triads is presented. The motivation of this paper is to formulate uniform solution procedures, pointing out the commonalities of various approaches and emphasizing a consistent method for synthesizing mechanisms defined by specified precision positions. Particular emphasis is given to the solution method using compatibility linkages. The textbook *Advanced Mechanism Design Vol II* by Erdman and Sandor (1984) only includes a small portion of the available information on this method, and several researchers have added to the basic knowledge in the years since. In some cases, the approach and nomenclature were not consistent, yielding a need to describe and chart a generic formulation and solution procedure for dyads/triads using compatibility linkages and solution structures. The present method offers benefits for solving for exact dyad/triad solutions for complex multiloop mechanisms and could be a promising tool for reducing the computational load of finding complex mechanisms, and for visualizing properties of the solution space.

Keywords: mechanism synthesis; compatibility linkages; Burmester curves

1. Introduction

The goal of synthesizing linkages and mechanisms to perform a particular task is a centuries-old practice. One famous example, called the South Pointing Chariot, was purportedly created by Chinese engineer Ma Jun (c. 200–265). As its name implies, a clever gear system driven by a chariot's wheels forces a statue on the back of the chariot to continually point south. This was true no matter how many turns the chariot took, provided both of its wheels rolled without slipping. This was a valuable navigational tool that significantly pre-dated the invention of the conventional magnetic compass [1,2]. However, for many centuries to follow, no formal or systematic methodology for synthesizing new mechanisms was developed.

Professor Robert Willis articulated this problem in the preface of his 1841 text "Principles of Mechanism" when he said, "By some strange chance, very few have attempted to give a scientific form to the ... results of mechanism; for it cannot be said that the few and simple ... examples in books of mechanics, are to be regarded as even forming a foundation ... that will enable us either to reduce the movements and actions of a complex engine to system or to give answers to the questions that naturally arise upon considering such engines" [3].

In the remainder of the text, Willis laid a foundation for later work and a challenge for mathematicians and engineers to create mathematical synthesis techniques. This call was taken up by the likes of Franz Reuleaux, James Watt, Ludwig Burmester, and Ferdinand Freudenstein. Each of them made a unique contribution to the field, such that by the early-mid 1900s, a mathematical basis for solving mechanism problems had been established.

The generations of kinematicians that followed more thoroughly fleshed out the techniques formulated by these early researchers, and developed more methods, such as

complex number and continuation methods. As the field has continued to expand, few centralized solution methodologies have arisen, but rather a collection of largely unique approaches that are mostly specific to the type of linkage topology.

There are many distinct ways to define problems, and, consequently, many distinct methods to solve them. Some define precision positions (x, y coordinates and relative angle) that a coupling link must pass through, some a path a single point must pass through, and others seek to generate vast sets of possible mechanism solutions through continuation methods [4–8]. Recent studies in kinematic synthesis have primarily emphasized algorithmic approaches.

For example, Purwar and Deshpande investigated a machine-earning approach to kinematic synthesis, with the intent of mitigating the solution mechanisms' sensitivity to the initial conditions [9]. In another paper, Baskar and Bandyopadhyay discuss an algorithm aimed at reducing the computational load of calculating the finite roots of large systems of polynomial equations, a problem that arose in kinematic synthesis as the mathematical method of polynomial continuation was implemented [10]. Ref. [11] demonstrates a procedure for synthesizing RR, PR or RP dyads, but using a blend of exact and approximate positions.

While evidently valuable, this paper leans away from these algorithm driven approaches in favor of more classical synthesis approaches that focus on directly solving the kinematic equations. Countless complex planar mechanisms can be formed by a combination of dyads and triads, which can be viewed as kinematic building blocks. As two examples, consider the multilink mechanisms shown in Figures 1 and 2. The first deploys the footrest of a chair, while the second moves the leading-edge flap of a wing into its working position. Both mechanisms are composed of multiple dyad and triad chains. Rather than attempting to develop a custom kinematic synthesis process for every complex linkage, a uniform strategy is preferred.
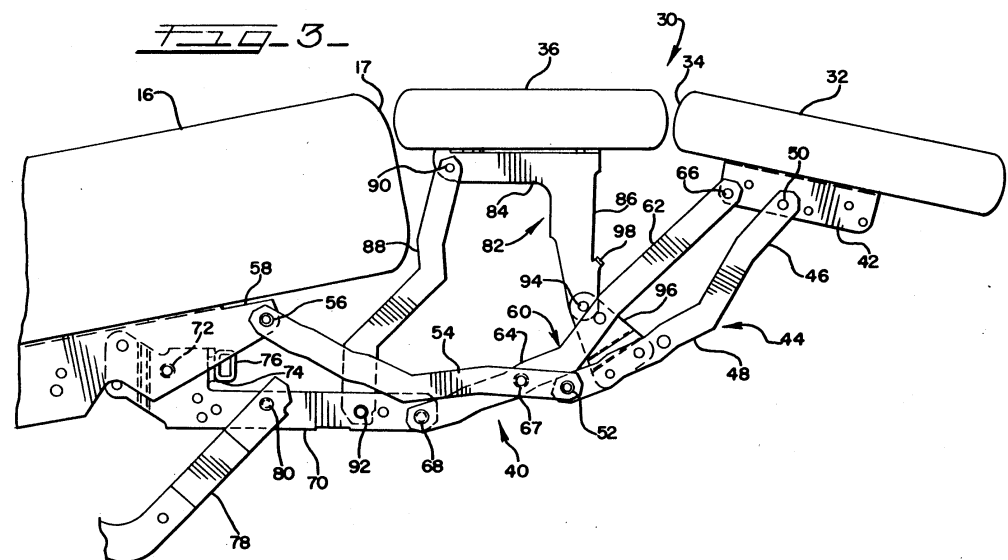

Figure 1. Patent figure of a chair with a deployable footrest [12].

Owing to some inherent properties of mechanisms and machines formed by links and joints, kinematic synthesis methods found in the literature share certain underlying mathematical principles that make finding one or more solutions possible. There exist a few analytical approaches to solving triad synthesis synthesis problems, some of which are analyzed in Reference [13], including a unique approach coined the "relative precision position approach for triad synthesis (p. 433)." Here, emphasis is placed on the solution method called the "compatibility linkage" for problems defined by precision positions. This method was first introduced by Sandor and Freudenstein [14] and summarized in Hartenberg, and Denavit [15] and later in Erdman and Sandor [4]. Further contributions

building on the foundation established by Sandor and Freudenstein were made by Chuen-Sen Lin and other authors [16–19].
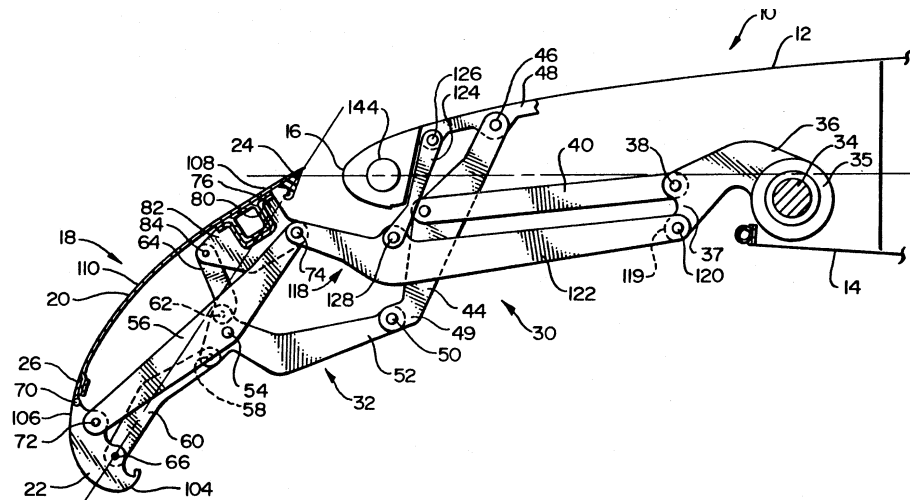

Figure 2. Patent figure of a leading edge flap of a wing [20].

2. Body

2.1. Precision Position Solution Methods

The starting point for using the complex number method for solving kinematic synthesis problems (defined by precision positions) is modelling the linkage mechanism using a number of "standard form equations" [4]. The equations are slightly different for a dyad and a triad. A dyad represents two links in the mechanism and has the form:

$$W\left(e^{i\beta_j} - 1\right) + Z\left(e^{i\alpha_j} - 1\right) = \delta_j \tag{1}$$

A triad represents three links in relative motion and has the form:

$$W\left(e^{i\alpha_j} - 1\right) + V\left(e^{i\beta_j} - 1\right) + Z\left(e^{i\gamma_j} - 1\right) = \delta_j - h_j \tag{2}$$

Note that W, Z, V, δ_j and h are vectors defined with complex numbers. Links in the mechanism that are not binary may be defined by more than one dyad or triad loop. These equations are illustrated in Figure 3a,b.

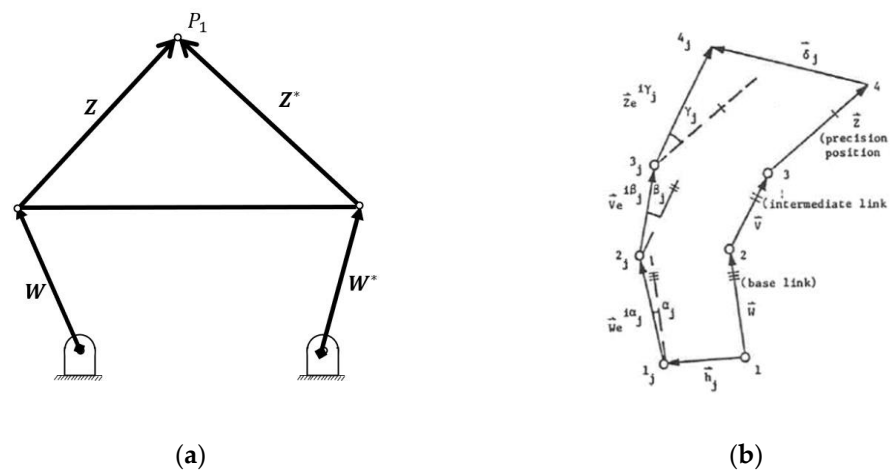

| (a) | (b) |

Figure 3. (**a**) The standard form depiction of a four-bar comprised two dyads. (**b**) The standard form depiction of a triad is shown in two positions. Reprinted with permission from ref. [21]. Copyright 1987 Chuen-Sen Lin.

Each of the terms on the left-hand side in the standard form equations represent a link (**W**, **V**, or **Z**) in an assembled mechanism. They are multiplied by rotational operators which represent the rotations of the link from the starting position to each prescribed position. The term δ_j represents the vector between the precision point in the i-th and j-th position (i.e., δ_2 goes between P1 and P2). In most cases, the terms δ_j and α_j are prescribed in the problem, and β_j is taken as a free choice. As the number of precision positions increases, the number of free choices that can be made decreases until there are no free choices left. As seen in Table 1, for problems involving a dyad in two or three positions, the number of free choices is such that the standard form equations can be solved with a linear solution, either directly or by Cramer's rule for a dyad in three positions. However, in the four-precision position case, there are three vector equations (six scalar equations) which must be solved simultaneously, but seven unknowns. As a result, a nonlinear solution method must be used. This is where the method of compatibility linkages is so useful.

Table 1. Maximum number of solutions for an unknown dyad/triad when δ_j and α_j are prescribed in the equation $W\left(e^{-i\beta_j}-1\right) + Z\left(e^{-i\alpha_j}-1\right) = \delta_j$ for dyads, and $W\left(e^{-i\alpha_j}-1\right) + V\left(e^{-i\beta_j}-1\right) + Z\left(e^{-i\gamma_j}-1\right) = \delta_j - h_j$ for triads.

Dyad/ Triad	Number of Positions	Number of Scalar Equations	Number of Scalar Unknowns	Number of Free Choices	Number of Solutions
Dyad	2	2	5	3	$O^{(\infty^3)}$
Dyad	3	4	6	2	$O^{(\infty^2)}$
Dyad	4	6	7	1	$O^{(\infty^1)}$
Dyad	5	8	8	0	Finite *
Triad	2	2	7	5	$O^{(\infty^5)}$
Triad	3	4	8	4	$O^{(\infty^4)}$
Triad	4	6	9	3	$O^{(\infty^3)}$
Triad	5	8	10	2	$O^{(\infty^2)}$
Triad	6	10	11	1	$O^{(\infty^1)}$
Triad	7	12	12	0	Finite *

* Solutions come in sets of 0, 2, or 4 for dyads, and sets of 0, 2, 4, or 6 for triads [4] (p. 94), [21] (p. 21).

Unlike the standard form dyad equation, the triad equation also includes the vector term h. This term adjusts the tail end of the vector chain, allowing for the solution method applicability even in completely ungrounded triad cases. The dyad equation can be modified to include the term h if required.

Figure 4 illustrates how a linkage system can be viewed as combinations of dyads and triads. Even though this six-bar is far less complex that the mechanisms shown in Figures 1 and 2, the following process can be applied to mechanisms with more loops and links in a similar way. For example, although a Stephenson III six-bar is shown, the other six-bar chains can be placed in the dyad-triad standard form as reported by Lonn [22].

The six-bar shown in Figure 4 has three loops, one dyad and two triads. They are defined by Equations (3)–(5) [4]. The first loop equation describes a dyad, while the next two describe triad loops.

$$Z_1\left(e^{i\varphi_j}-1\right) + Z_2\left(e^{i\gamma_j}-1\right) = \delta_j \tag{3}$$

$$Z_5\left(e^{i\psi_j}-1\right) + Z_4\left(e^{i\beta_j}-1\right) - Z_3\left(e^{i\gamma_j}-1\right) = \delta_j \tag{4}$$

$$Z_6\left(e^{i\theta_j}-1\right) + Z_7\left(e^{i\beta_j}-1\right) - Z_3\left(e^{i\gamma_j}-1\right) = \delta_j \tag{5}$$

Using free choices of link vectors, this mechanism can be solved with three dyads [4] (p. 113). Ref. [4] has other examples of assigning dyad and triad standard form modelling to multiloop mechanisms including an eight bar with four triads and geared mechanisms. Once a linkage system is modelled with combinations of dyad and triad standard form equations, the compatibility linkage solution process is used to reveal the potential solution space.
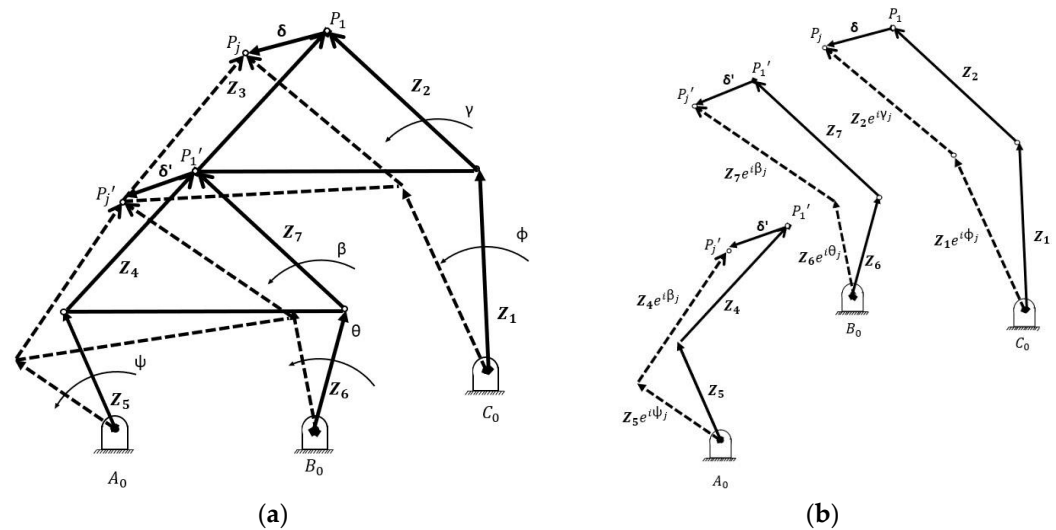

Figure 4. (**a**) A multiloop mechanism shown in an assembled form. (**b**) The same multiloop mechanism decomposed into three components, two triads and one dyad.

A practical mechanism which reveals these loops can be seen in Figure 5a, with the loops shown in Figure 5b. The mechanism guides a rotor on a drone from a vertical position into a horizontal position, allowing for the same rotor to produce vertical or forward thrust. This setup would allow for the drone to takeoff vertically but fly in a typical "fixed-wing" configuration once in the air, improving its efficiency. This particular example is very challenging due to significant constraints on both the ground and moving pivots. The ground pivots must both be within the nacelle, and the moving pivots are very close to the link holding the propellor. In addition, the mechanism must deploy smoothly without exhibiting poor transmission angles. The dimensional synthesis resulted in the Z values shown in Table 2.
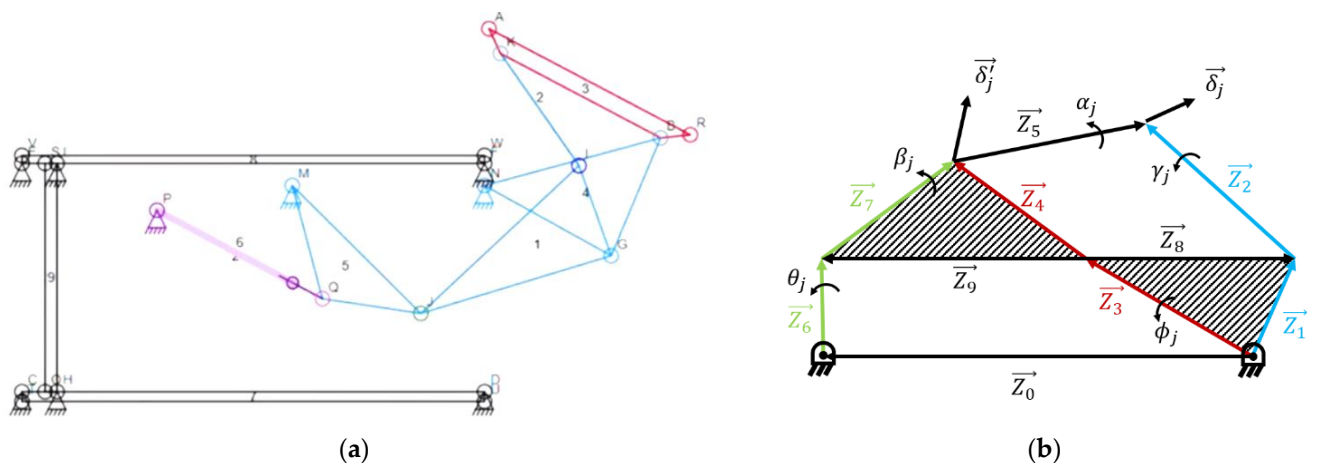

Figure 5. (**a**) The synthesized Watt 1 multiloop mechanism for guiding a drone rotor out of the nacelle and into a vertical position [23,24]. (**b**) The breakdown of the vector loops comprising the Watt 1 mechanism [23].

Table 2. Synthesized Z-Vectors.

Link	Vector (PP1)
Z_0	$-3.377 + 0i$
Z_1	$0.405 - 3.178i$
Z_2	$0 + 3.178i$
Z_3	$-1.522 - 2.037i$
Z_4	$-0.436 + 1.620i$
Z_5	$2.364 + 0.416i$
Z_6	$-1.560 - 2.773i$
Z_7	$2.978 + 2.357i$
Z_8	$1.927 - 1.141i$
Z_9	$-3.170 - 0.684i$

A proof-of-concept prototype was assembled, seen in Figure 6.
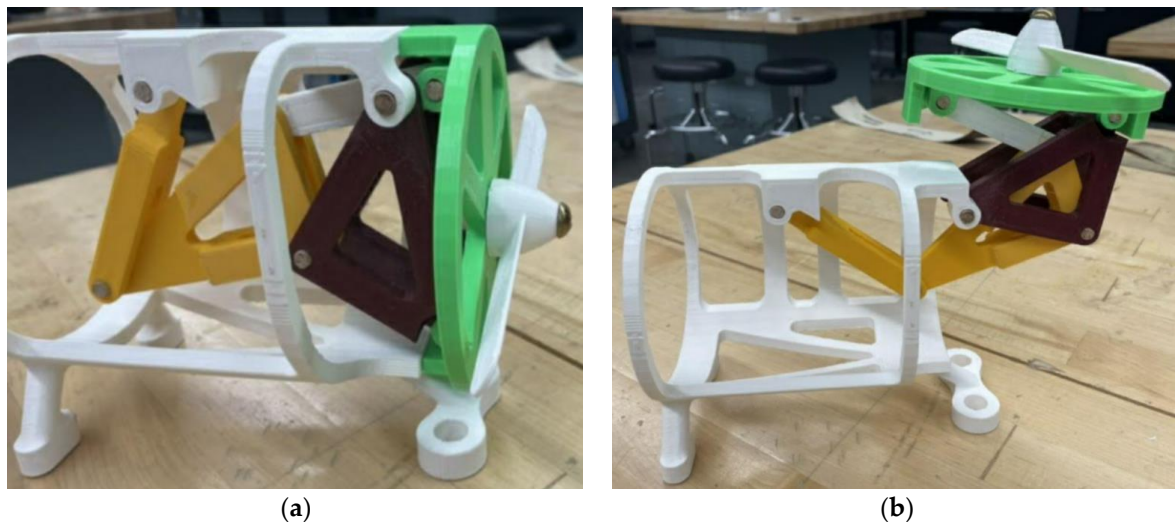

(**a**)　　　　　　　　　　　　　　　(**b**)

Figure 6. (**a**) A 3D printed prototype in the initial "fixed-wing" position [23]. (**b**) The prototype in the open, vertical liftoff configuration.

2.2. Compatibility Linkage Solution Procedure, Dyad for 4 Precision Points

The purpose of the compatibility linkage is to find "compatible values" of several unknown variables in a set of nonlinear synthesis equations that are compatible with the known or specified variables. This method results in a closed-form solution to these equations. The compatibility linkage technique, which was introduced by Sandor and Freudenstein [14], takes advantage of insights gained by graphical and analytical precision position methods—both approaches provide keys to generating solutions for triads and dyads.

As with other precision position methods, it is assumed that the designer has either determined or measured the required x and y locations, and angles, of the precision point in each position, meaning that $\delta_{i\text{-}j}$ and $\alpha_{i\text{-}j}$ are known. Depending on the number of positions being considered for a particular problem, the designer may have additional free choices to make, but the change in position coordinates and angle between positions should always be known.

The compatibility linkage general solution procedure will be emphasized and illustrated with a planar dyad. The first step is to translate the known information into the standard form vector equations [4,12] (see Equations (1) and (2)). As seen in Figure 3, each

vector **W**, **Z**, (and for triads, **V**), represents a link in a dyad or triad. Note that the two links **Z** and **Z′** shown in Figure 3a do not represent two unique links, but rather two vectors embedded in the same link.

The number of standard-form equations should be one less than the number of precision positions selected in the problem. The only terms that change in each of these equations are the angles β_j, α_j, γ_j, and the vector δ_j for each additional position j. These equations are then translated into a matrix form, which looks like this:

$$\begin{bmatrix} e^{i\beta_2} - 1 & e^{i\alpha_2} - 1 \\ e^{i\beta_3} - 1 & e^{i\alpha_3} - 1 \\ e^{i\beta_4} - 1 & e^{i\alpha_4} - 1 \end{bmatrix} \begin{bmatrix} W \\ Z \end{bmatrix} = \begin{bmatrix} \delta_2 \\ \delta_3 \\ \delta_4 \end{bmatrix} \qquad (6)$$

[4] (p. 180).

This equation will look roughly the same for a triad, except a column is added for **V** in the first matrix, and **V** is added to the column vector **WVZ**. An augmented matrix can be formed by adding the column vector δ_{2-4} to the matrix on the left-hand side. A known property of this type of system is that a solution only exists if the rank of the augmented matrix is two (for a dyad in four positions), with rank referring to the number of linearly independent rows in the matrix. The rank can be most easily checked by finding the determinant of the matrix. For square matrices such as the augmented matrix under consideration, if the determinant equals zero, the rank of the matrix is based on the non-zero cofactor (also called minor in math) of the maximum possible order [25]. The following expressions are derived from these properties.

$$Det\ M = Det \begin{bmatrix} e^{i\beta_2} - 1 & e^{i\alpha_2} - 1 & \delta_2 \\ e^{i\beta_3} - 1 & e^{i\alpha_3} - 1 & \delta_3 \\ e^{i\beta_4} - 1 & e^{i\alpha_4} - 1 & \delta_4 \end{bmatrix} = 0 \qquad (7)$$

[4] (p. 181).

This determinant can be written into the following expression, known as the compatibility equation:

$$\mathbf{\Delta_2} e^{i\beta_2} + \mathbf{\Delta_3} e^{i\beta_3} + \mathbf{\Delta_4} e^{i\beta_4} + \mathbf{\Delta_1} = 0 \qquad (8)$$

[4] (p. 181).

where each vector $\mathbf{\Delta_{2-4}}$ is the cofactor matrix associated with the corresponding β value in the augmented matrix. The cofactors are found by eliminating the row and column containing each value of β, as follows (e.g., $\mathbf{\Delta_2}$):

$$\begin{bmatrix} \cancel{e^{i\beta_2} - 1} & \cancel{e^{i\alpha_2} - 1} & \cancel{\delta_2} \\ \cancel{e^{i\beta_3} - 1} & \begin{bmatrix} e^{i\alpha_3} - 1 & \delta_3 \\ \cancel{e^{i\beta_4} - 1} & e^{i\alpha_4} - 1 & \delta_4 \end{bmatrix} \end{bmatrix} \qquad (9)$$

The cofactor matrix formed from what remains after eliminating this row and column is marked in the gray box. For a dyad in four positions, the cofactor matrices are given as follows:

$$\mathbf{\Delta_2} = \begin{vmatrix} e^{i\alpha_3} - 1 & \delta_3 \\ e^{i\alpha_4} - 1 & \delta_4 \end{vmatrix} \qquad (10)$$

$$\mathbf{\Delta_3} = - \begin{vmatrix} e^{i\alpha_2} - 1 & \delta_2 \\ e^{i\alpha_4} - 1 & \delta_4 \end{vmatrix} \qquad (11)$$

$$\mathbf{\Delta_4} = \begin{vmatrix} e^{i\alpha_2} - 1 & \delta_2 \\ e^{i\alpha_3} - 1 & \delta_3 \end{vmatrix} \qquad (12)$$

[4] (p. 181).

Note that for dyads, the cofactor matrices will always be 2 × 2, while for triads, the cofactor matrices will be 3 × 3. Additionally, each of the vectors $\mathbf{\Delta_{2-4}}$ is a matrix signified

with vertical lines rather than conventional matrix brackets. This is a mathematical short-hand representing a determinant, meaning that each of these terms (once the determinant is evaluated) is a vector with a magnitude and direction. The term $\boldsymbol{\Delta_1}$ is unique from the others, defined by the following expression:

$$\boldsymbol{\Delta_1} = -\boldsymbol{\Delta_2} - \boldsymbol{\Delta_3} - \boldsymbol{\Delta_4} \tag{13}$$

[4] (p. 181).

As brilliantly noted in [14], this equation can be viewed as a four link mechanism in its starting position—thus named the compatibility linkage. Equation (13) is the equation of closure where $\boldsymbol{\Delta_1}$ is the fixed link and the rest of the vectors close the loop by connecting the chain's head to its tail. Plotting each of the four above vectors without applying any of the beta rotation angles mathematically will resemble Figure 7 (for a dyad in four positions, see Table 3 for more configurations).
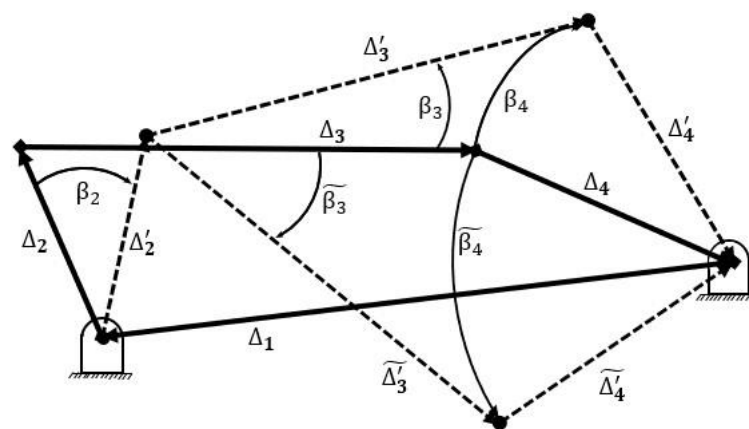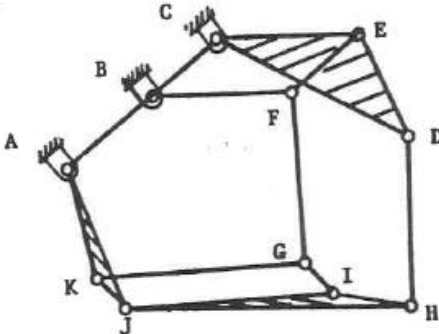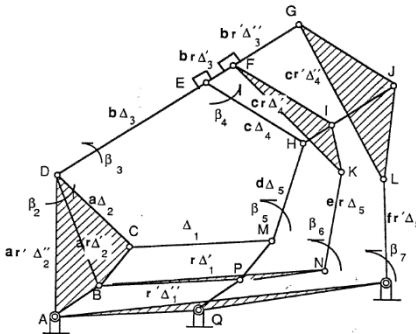

Figure 7. The compatibility linkage for a dyad in four precision positions. The resultant position of each link is shown after applying a rotation of β_2. There are two combinations of the links $\boldsymbol{\Delta_3}$ and $\boldsymbol{\Delta_4}$ which close the linkage. Both represent a viable solution to the original problem for the given value of β_2.

Table 3. Summary of the solution process for compatibility linkages for dyads and triads.

Dyad/ Triad	Number of Positions	Number of Links	Number of Cofactor Matrices	Procedure	Compatibility Linkage BKC
Dyad	4	Four-bar compatibility linkage	4; Δ_1, Δ_2, Δ_3, Δ_4	1. Write standard form equations, put them in an augmented matrix form, write the cofactor matrices 2. Create Δ_1 as the sum of Δ_{2-4}, then draw the linkage. 3. Rotate Δ_2 by β_2, rotate Δ_3 and Δ_4 to close the loop. 4. Read off the angular displacement of Δ_3 and Δ_4 to get β_3 and β_4.	
Dyad	5	Seven—bar structure, six-bar compatibility linkage	7; Δ_1, Δ_2, Δ_3, Δ_4, Δ_1', Δ_2', Δ_3'	1. Write standard form equations, put them in an augmented matrix form, write the cofactor matrices. There are two sets, Δ and Δ'. 2. Using a consistent scale, plot both complete loops, with the base of the Δ_1 links at the same x, y position 3. Rotate either loop until Δ_2 and Δ_2' are colinear. 4. Form a parallelogram about the Δ_3 links, creating point D. 5. Remove the newly formed link DE to find the final compatibility linkage. 6. Rotate Δ_2 by β_2, adjusting other links accordingly. Positions where BE and CD are parallel represent solutions.	 [21] (p. 109)
Triad	5	Five-bar 2-DOF compatibility linkage	5; Δ_1, Δ_2, Δ_3, Δ_4, Δ_5	Repeat steps 1–4 of the dyad in 4PP. The difference is that the loop has five links instead of four, so the designer will need to set two free choices, typically the angles of Δ_2 and Δ_5.	 [21] (p. 113)

Table 3. *Cont.*

Dyad/ Triad	Number of Positions	Number of Links	Number of Cofactor Matrices	Procedure	Compatibility Linkage BKC
Triad	6	Eleven-bar structure, ten-bar compatibility linkage	9; Δ_1, Δ_2, Δ_3, Δ_4, Δ_5, Δ_1', Δ_2', Δ_3', Δ_4'	Repeat steps 1–6 for the dyad in five positions. In the example at right, Δ_3 is used as the ground pivot. There are two parallelogram loops to form in step four. One about Δ_4, forming BCEF, and one about Δ_1, forming GIJK. Remove a link from either parallelogram to convert to the compatibility linkage.	[21] (p. 35)
Triad	7	Fifteen-bar structure, fourteen-bar compatibility linkage	13; Δ_1, Δ_2, Δ_3, Δ_4, Δ_5, Δ_1', Δ_2', Δ_3', Δ_4', Δ_1'', Δ_2'', Δ_3'', Δ_4''	Repeat steps 1–6 for the dyad in five positions. There are several parallelogram loops to form in step four. Loops should be formed between each layer of the linkage. Here, they are formed about Δ_4 and Δ_1, and the layers of link Δ_2 are fused to form a single link. Remove a link from any parallelogram to convert to the compatibility linkage *.	[21] (p. 117)

* Additional information regarding the solution procedure for a triad in six and seven precision positions is shown in Appendix A, including a simplified form of the six-precision position compatibility linkage.

One frequent point of confusion is that the compatibility linkage is related to the actual solution dyad. This is not the case. Rather, the constructed compatibility linkage is only the tool to allow the user to find compatible solutions for the unknown angles in the standard form equations.

Once the linkage is assembled, the user applies a rotation of β_2 to link Δ_2. Consequently, the links for Δ_3 and Δ_4 need to translate and rotate by some amount to keep the loop closed, as Δ_1 is considered ground, and does not move. Once solved, the displacement angles of links Δ_3 and Δ_4 represent the solution values of β_3 and β_4. These values are then plugged into the original standard form dyad equations. With β_3 and β_4 identified, solving for the vectors W and Z using standard linear algebra techniques is possible.

While the problems may be a bit more complex, increasing the number of precision positions or transitioning from a dyad to a triad changes very little about the underlying methodology for compatibility linkages. While this paper will not emphasize quadriads, it is even possible to apply the method of compatibility linkages to solving four link chains [21]! Here, each higher-order case up to seven precision positions will be briefly examined, highlighting the key differences of each from the dyad in four positions explained above. See Table 3 for a summary of these cases and see Appendix A for a detailed solution procedure of the triad in six and seven positions.

2.3. Dyad in 5 Precision Positions

Moving from four to five positions is likely the biggest single jump in complexity for solving problems using the method of compatibility equations. This is because there is no longer a single compatibility equation, but rather two. The compatibility equations for a dyad with five prescribed positions (no free choices) are:

$$\begin{vmatrix} e^{i\beta_2} - 1 & e^{i\alpha_2} - 1 & \delta_2 \\ e^{i\beta_3} - 1 & e^{i\alpha_3} - 1 & \delta_3 \\ e^{i\beta_4} - 1 & e^{i\alpha_4} - 1 & \delta_4 \end{vmatrix} = 0 \tag{14}$$

and

$$\begin{vmatrix} e^{i\beta_2} - 1 & e^{i\alpha_2} - 1 & \delta_2 \\ e^{i\beta_3} - 1 & e^{i\alpha_3} - 1 & \delta_3 \\ e^{i\beta_5} - 1 & e^{i\alpha_5} - 1 & \delta_5 \end{vmatrix} = 0 \tag{15}$$

[4] (p. 201).

Or, in their simplified form:

$$\Delta_2 e^{i\beta_2} + \Delta_3 e^{i\beta_3} + \Delta_4 e^{i\beta_4} + \Delta_1 = 0 \tag{16}$$

$$\Delta'_2 e^{i\beta_2} + \Delta'_3 e^{i\beta_3} + \Delta_4 e^{i\beta_5} + \Delta'_1 = 0 \tag{17}$$

[21] (p. 107) where

$$\Delta_1 = -\Delta_2 - \Delta_3 - \Delta_4 \tag{18}$$

$$\Delta'_1 = -\Delta'_2 - \Delta'_3 - \Delta_4 \tag{19}$$

The Δ' terms are formed in the same way as the Δ terms (cofactors of the augmented matrix), but they are taken from the second matrix. These equations must be fulfilled simultaneously to find a valid solution for W and Z. Previously, finding the solution to these compatibility equations would have required using a technique known as "Sylvester's Dyalitic Eliminant". While this method worked, the process is computationally involved and mathematically rigorous. Using the method of compatibility linkages described below allows the designer to avoid this complexity while being able to visualize the solution process.

To form a solution structure, identify each of the two independent four-bar loops formed by the Δ terms. The first loop includes Δ_1 through Δ_4, while the second is formed from Δ_1', Δ_2', Δ_3', and Δ_4 (Δ_4 used twice because Δ_4' is identical to it, either notation is acceptable). Using a consistent scale, line up these two four bars such that the tails of

Δ_2 and Δ_2' share the same x, y coordinate, and rotate either four-bar linkage (keeping all internal angles the same) such that Δ_2 and Δ_2' have the same angular direction. The result should now resemble Figure 8, with Δ_1 (A-G-H) and Δ_2 (A-B-C) appearing as ternary links. There are two distinct four-bar chains, or loops, between them.
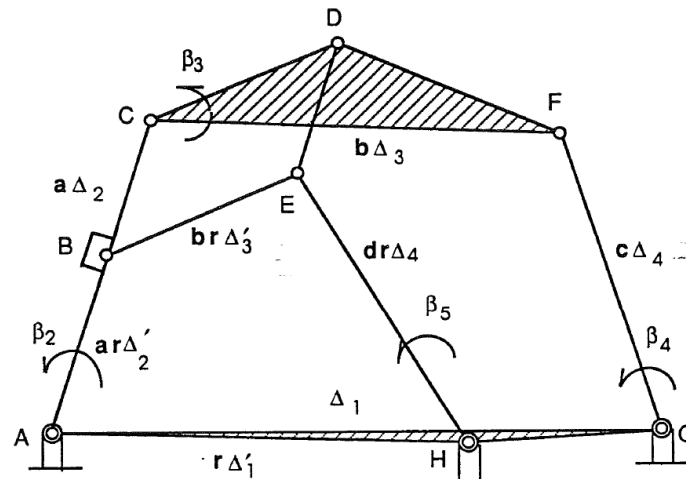

Figure 8. The compatibility linkage for a dyad in five precision positions. Linkage positions in which the lines CD and BE are parallel represent solutions to the synthesis problem [21] (p. 109).

The final key step shown in Figure 8 is adding point D. This point is found by creating the parallelogram BCDE, turning link CF (corresponding to Δ_3) into a ternary link. The completed mechanism is known as the solution structure. Once identified, the link DE may be removed, but point D will remain as a reference. After removing link DE, the mechanism transforms from a zero degree-of-freedom structure to a one degree-of-freedom linkage; this is the final compatibility linkage.

To find solutions, rotate the (now ternary) link Δ_2. The rotation of Δ_2 is the only input required to fully define the system, so each other link is determined once the angle of Δ_2 is set. As this mechanism moves, at any position where the links CD and BE are parallel, the linkage represents a compatible solution to the original problem. The exception is the first position, as CD and BE will always be parallel initially, by definition.

For each unique parallel position, the displacement angles of the links correspond to the angles β_{2-5}. Specifically, $\angle\Delta_3 = \beta_3$, $\angle\Delta_4$ (outer loop)$= \beta_4$, and $\angle\Delta_4$ (inner, Δ' loop)$= \beta_5$. These compatible angles are then inserted back into the standard form dyad equations. With four vector equations and two vector unknowns, the equation can now be solved for W and Z via a linear solution. The number of geometric inversions of the compatibility linkage corresponds to the number of solution sets to the compatibility equations. The term geometric inversion refers to the number of unique mechanisms that can be created by changing which link is fixed, meaning distinct inversions do not have unique angular displacements, just different grounded links. In this case, that means there are six sets of unique combinations of β_{2-5} which fulfill the original compatibility equations. However, two of these solutions correspond to the slider and concurrency special points. As a result, only up to four dyad solutions exist—that is, there are zero, two or four viable solutions for each choice of independent variable x.

2.4. Triad in 5 Precision Positions

As a designer transitions from synthesizing a dyad to a triad, the underlying solution procedure will remain the same, but a few key steps will either change or be added. First, the standard triad equation has an additional term, $e^{i\gamma j}-1$, associated with the Z vector. See Figure 3b depicting the vector form of a triad to see where this term fits in the vector chain. Similarly, an intermediate vector V has been added, increasing the number of links in the chain from two to three. The meaning of some of the angles have changed as well. The

angle α no longer describes the angle of the coupler link, but rather the angle of the vector **W**. β is now assigned to the intermediate link **V** and will continue to be selected as the free choice for these problems. The new angle, γ, replaces α as the angle describing the coupler's rotation. It is important to note that using triads instead of dyads for five precision positions does not increase the number of loops in the compatibility linkage—there is still only a single loop—but the triad does increase the number of terms that must be identified. All values of γ must also be prescribed along with all the information that was prescribed for a dyad in five positions. This volume of free choices enables a designer to make many decisions about their desired mechanism, but this can also be overwhelming due to the vast potential solution space. For the triad in five positions, there are four simultaneous vector equations, and one compatibility equation:

$$\mathbf{\Delta_2}e^{i\beta_2} + \mathbf{\Delta_3}e^{i\beta_3} + \mathbf{\Delta_4}e^{i\beta_4} + \mathbf{\Delta_5}e^{i\beta_5} + \mathbf{\Delta_1} = 0 \tag{20}$$

[21] (p. 111)

$$\mathbf{\Delta_1} = -\mathbf{\Delta_2} - \mathbf{\Delta_3} - \mathbf{\Delta_4} - \mathbf{\Delta_5} \tag{21}$$

As with the compatibility linkage for a dyad in four positions, only one compatibility equation exists for a triad in five positions. As a result, the compatibility equation only has a single loop. However, one significant difference between the two is the additional link in the five-bar compatibility equation. This results in a solution structure with two degrees of freedom rather than one. However, this challenge can be avoided by giving the designer a second free choice. Typically, these free choices are chosen as β_2 and β_5, though any other combination of two angles is also valid. Once these free choices are made, the solution procedure is the same as the dyad in four positions, as all that is left is a geometrically deterministic triangle. The remaining link positions and angles can be solved by using the law of cosines. Table 3 and Figure 9 represent summaries of the dyad and triad solution procedures using the compatibility linkage approach. The similarities across these cases are indicated, perhaps suggesting a future software kinematic synthesis package. One example in this direction was achieved by Chase [26], although there was limited use of this software at that time.

A full explanation of the solution procedure using the compatibility linkage for a triad in six and seven precision positions can be found in Appendix A. While kinematic chains above dyads and triads will not be discussed in detail here, Lin demonstrated the general solution procedure for the compatibility linkage of a quadriad [21]. Theoretically, even higher-order chains also ought to be solvable by compatibility linkages. However, it becomes increasingly difficult to fathom a sufficiently complex yet practical mechanism synthesis problem that would justify their use. Even so, chains incorporating five or more vectors/links, and their potential applications, remain a possible area for further study.
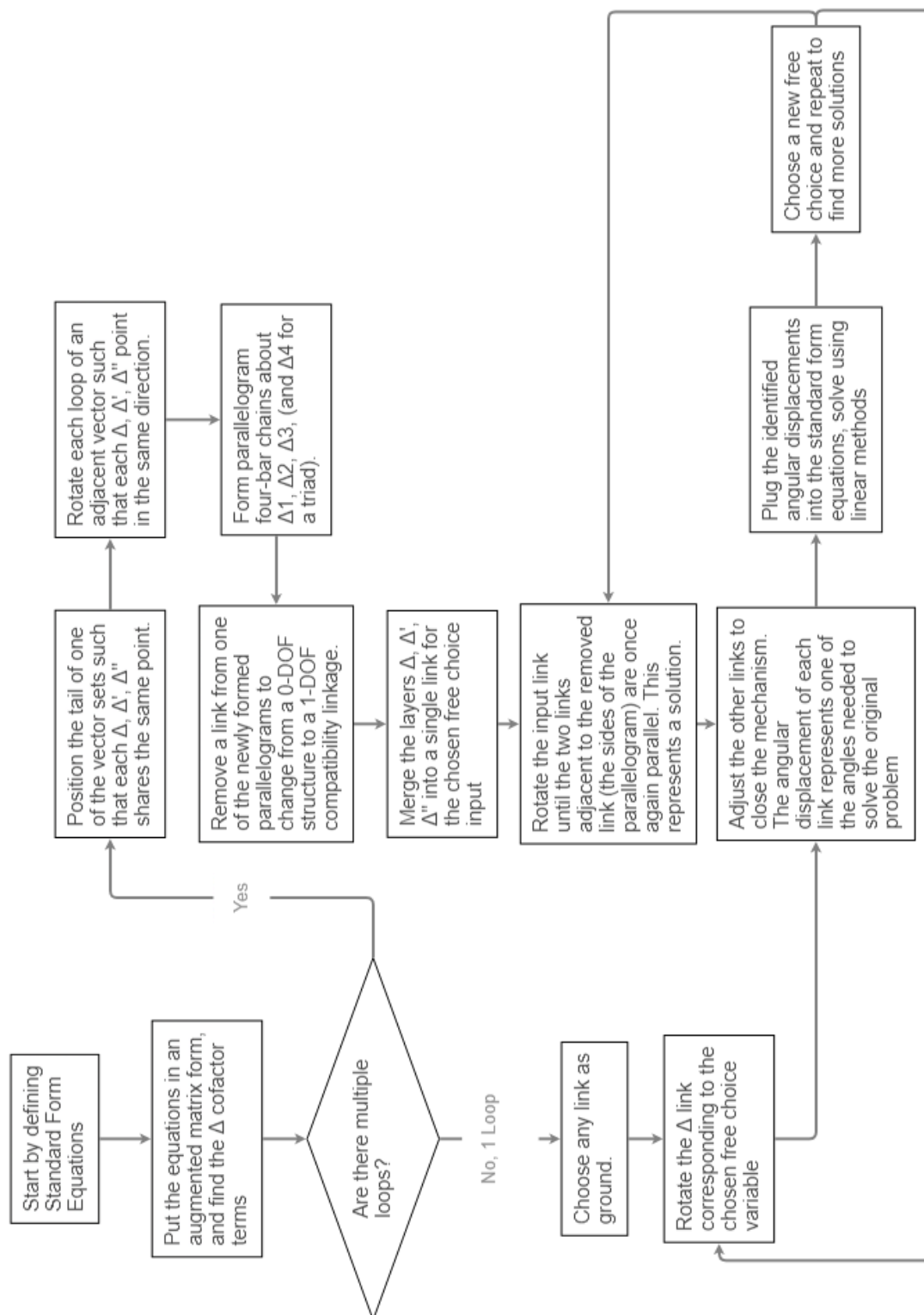
Figure 9. General solution procedure flow chart.

2.5. General Solution Procedure

A flow chart is provided in Figure 9 depicting the general solution procedure using the method of compatibility linkages. Inspiration for the chart comes from [21] (pp. 140–143).

To solidify the general solution procedure, the authors find it prudent to provide the following numerical example, a dyad in five precision positions. The problem is defined by the precision positions stated in Table 4.

Table 4. Precision positions and alpha angles.

Position	Coordinates	Alpha (deg)
1	$-21.700 + 22.035i$	0
2	$-11.883 + 12.018i$	19.684
3	$-5.973 + 11.767i$	30.751
4	$4.744 + 10.766i$	59.361
5	$5.345 + 12.318i$	84.696

Using Equations (7)–(13) and (19), the vectors representing the links in the compatibility linkage are found, shown in Table 5. These vectors form two four-bar loops, shown in Figure 10. The end of vector Δ_1 is chosen as the shared point between the two loops.

Table 5. Direction and magnitude of each Δ vector.

Delta Link	Vector Coordinates
Δ_1	$-1.2736 + 0.1990i$
Δ_2	$0.9214 - 3.4612i$
Δ_3	$1.5541 + 3.7924i$
Δ_4	$-1.2018 - 0.5302i$
$\Delta_1{}'$	$-3.3851 + 1.1261i$
$\Delta_2{}'$	$5.2149 - 9.7840i$
$\Delta_3{}'$	$-0.6280 + 9.1881i$
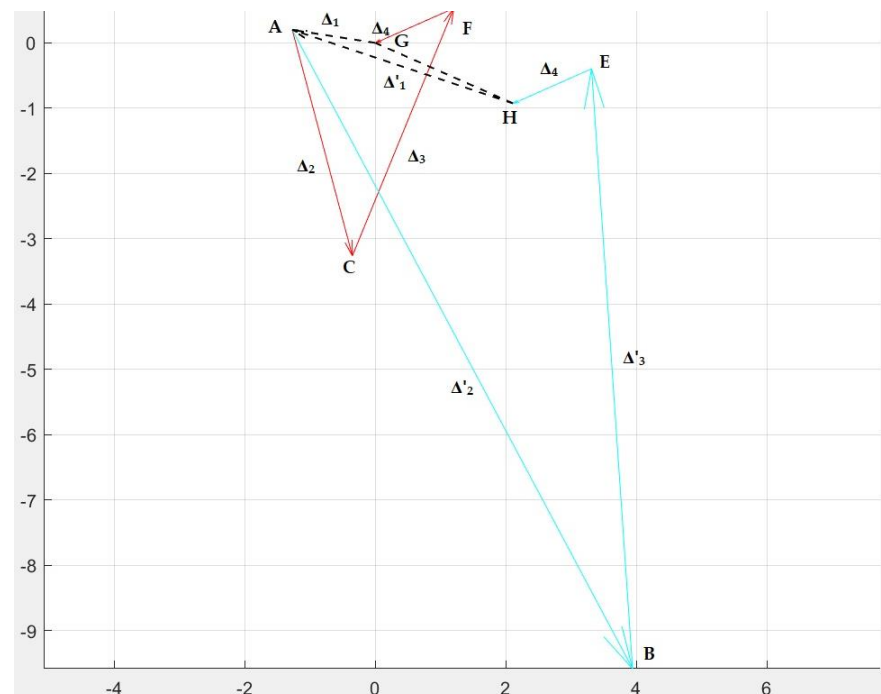
Figure 10. The unmodified plot of the Δ vectors for a dyad in five precision positions.

At this point, the links Δ_2 and $\Delta_2{}'$ are chosen as the input which will drive the compatibility linkage. As a result, all of the Δ' links are rotated about the head of vector Δ_1 to align Δ_2 and $\Delta_2{}'$ so that they are colinear, a rotation of -13.15 degrees (CW). Additionally, a parallelogram is formed by drawing a vector from the end of $\Delta_3{}'$ in the direction of Δ_2.

This vector has length $\boldsymbol{\Delta_2} - \boldsymbol{\Delta_2}'$=1.9307 − 7.2528i. After applying these changes, the compatibility linkage takes the form shown in Figure 11.
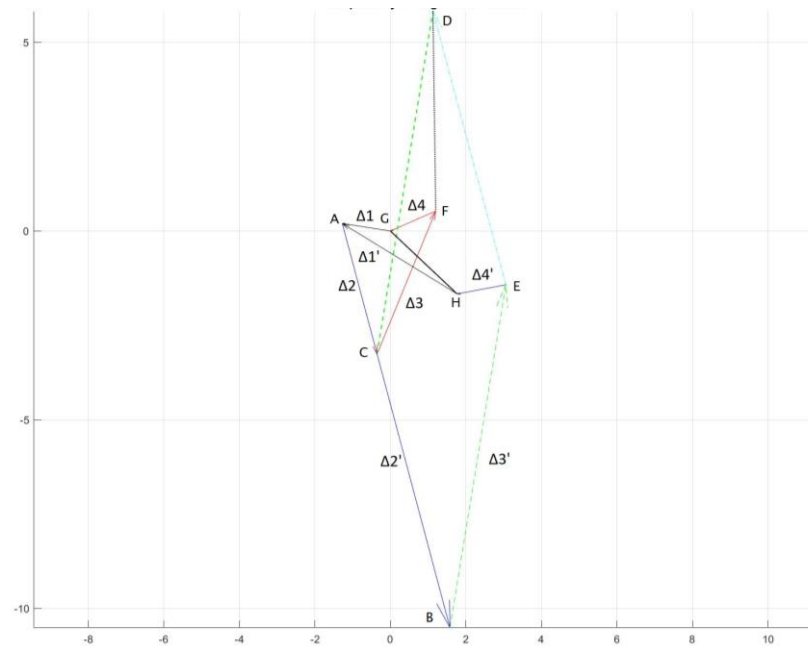

Figure 11. The solution structure for a dyad in five precision positions.

Figure 11 is the solution structure representing this problem. Removing the link DE forms the compatibility linkage. To use it, the designer can directly begin rotating the linkage to try to find solutions. However, a useful intermediate step is to find the range of acceptable β_2 values for which the compatibility linkage closes. This range is found by drawing a circle with radius $\boldsymbol{\Delta_2}$ around the tip of $\boldsymbol{\Delta_1}$, as well as a circle of radius $|\boldsymbol{\Delta_2}|$ + $|\boldsymbol{\Delta_3}|$ + $|\boldsymbol{\Delta_4}|$ around the tail of $\boldsymbol{\Delta_1}$. Repeat this process for the $\boldsymbol{\Delta'}$ loop. Here the range of the $\boldsymbol{\Delta}$ loop is more limiting. The range of $\boldsymbol{\Delta_2}$ is shown in Figure 12, with the circle's intersections denoting the limits of $\boldsymbol{\Delta_2}$.
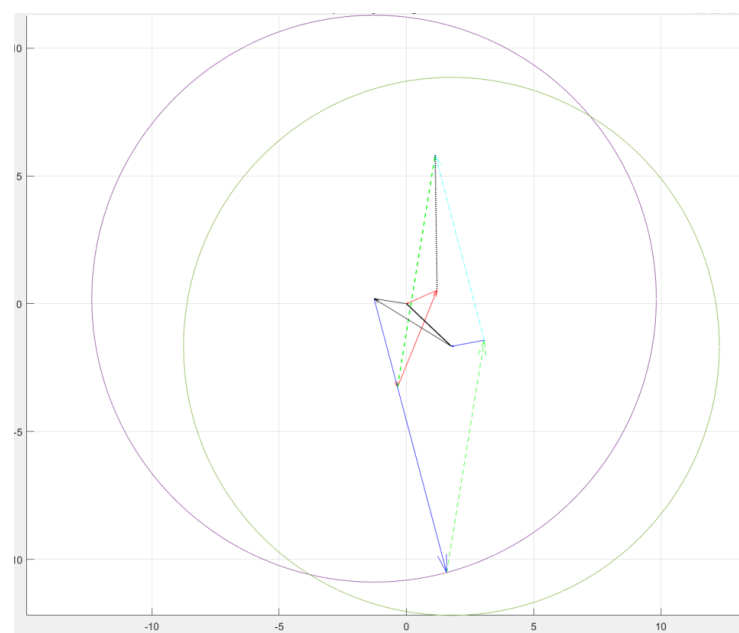

Figure 12. Procedure for finding the range of β_2. Here the two intersections of the circles represent the upper and lower bound of the angle.

From these circle intersections, it is possible to calculate an upper and lower bound of β_2 as 116 degrees above the initial position (CCW), and 27 degrees below the initial position (CW). The mechanism is rotated over this range, and any positions where links CD and BE are parallel to each other is recorded. In this problem, there are two such positions, shown in Figure 13a,b.
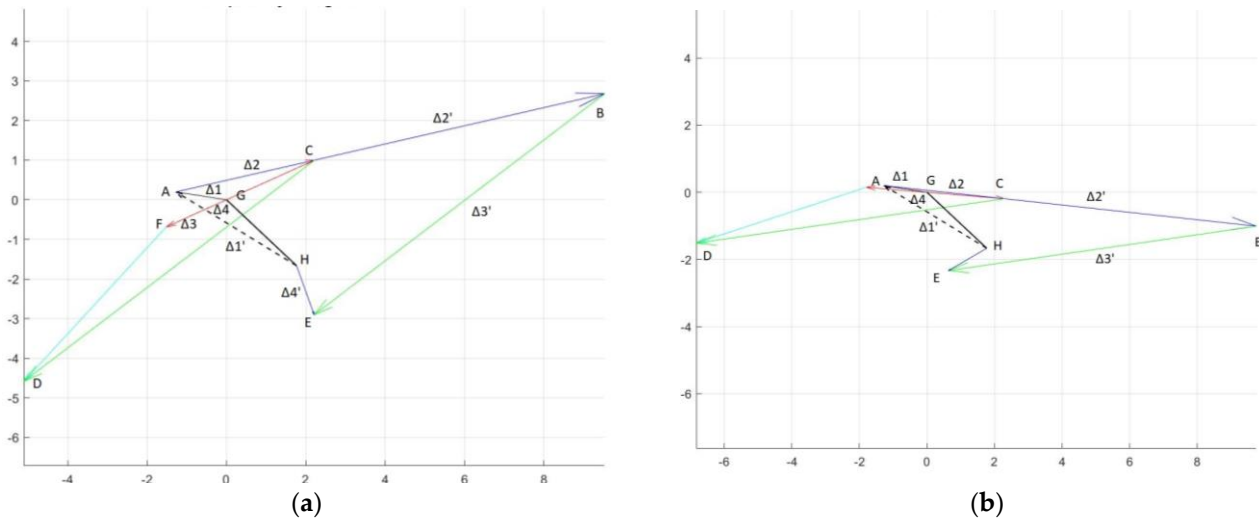

Figure 13. (**a**) Compatibility linkage in solution position one. (**b**) Compatibility linkage in solution position two.

In each of these two compatibility linkage positions, the links are measured to determine their angular displacement relative to the initial position. From these displacements, two dyads are found, corresponding to two solution positions, by plugging the values back into the standard form equations and finding a linear solution. These two dyads are plotted using the software Lincages in Figure 14 [27,28].
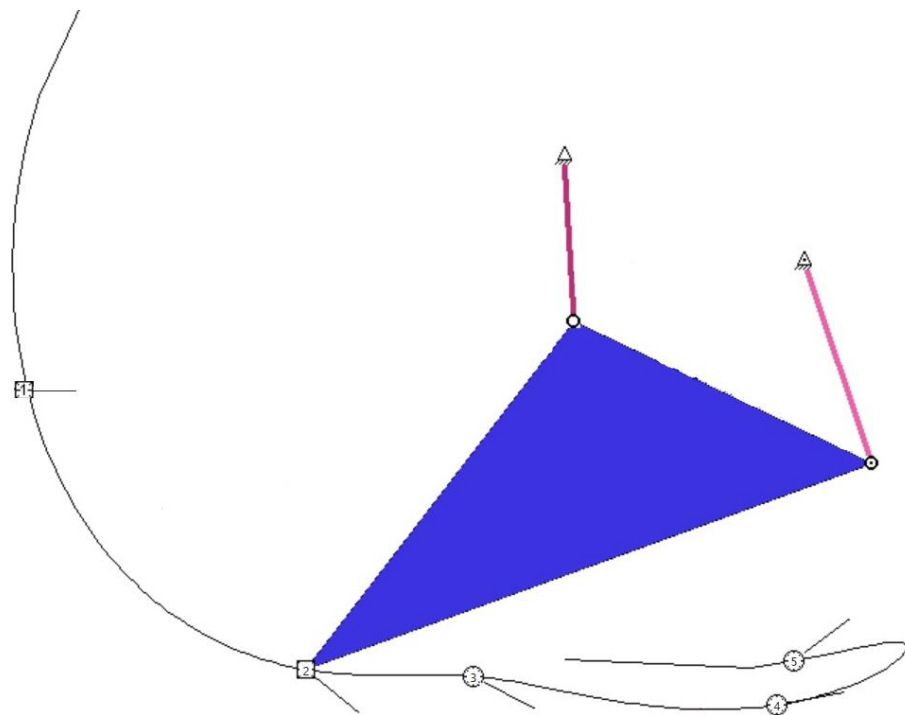

Figure 14. Final solution linkage visualized in the Lincages software. The triangles represent the ground pivots of this mechanism.

2.6. Special Cases

As with other synthesis methods, there are several special cases when solving problems using the compatibility linkage. A few of the most common will be emphasized here, and Figure A4 shows a more complete table of special cases.

The first set of special cases occurs when the free choice angle β_2 is equal to α_2, γ_2, or 0. This results in Equation (2) taking the form shown in Equation (22) (for $\beta_2 = \alpha_2$). Each of these cases is resolved by the solution containing a slider.

$$\boldsymbol{W}\left(e^{i\alpha_j} - 1\right) + \boldsymbol{V}\left((p_j)e^{i\alpha_j} - 1\right) + \boldsymbol{Z}\left(e^{i\gamma_j} - 1\right) = \delta_j - h_j \tag{22}$$

In this solution case, all angle variables are predefined prior to performing any calculations. The only scalar term which is not defined is p_j. p_j is called the stretch factor, and p_2 is the free choice for this problem.

The second set of special cases is also caused by other angular similarities. They are: one link with no angular displacement (i.e., $\alpha_j = 0$), two links with the same angular displacement (i.e., $\alpha_j = \gamma_j$), and multiple links with no angular displacement (i.e., $\alpha_j = \gamma_j = 0$). Each of these special cases is resolved through some combination of sliders, with the exception of $\gamma_j = 0$, for which no solutions exist. For a full depiction of the special cases for triads, see Figure A4.

2.7. Advantages of the Compatibility Linkage Method

By analyzing a compatibility linkage for range of rotation of the "input link" of the compatibility linkage, some interesting properties of possible solution mechanisms are revealed. Frequently, the link $\boldsymbol{\Delta_2}$ will have a finite rotational range, meaning that only values of β_2 falling in the acceptable range can produce solutions. This is quite useful, as previously, the range of acceptable β_2 (free choice) values would have been found through an exhaustive search. Through the method of compatibility linkages, the designer can clearly identify the upper and lower bounds of β_2 based on how far link $\boldsymbol{\Delta_2}$ in the compatibility linkage will rotate in either direction from its starting position. For example, a crank-rocker type compatibility linkage will give β_2 a range that allows any value to be used as a free choice. In contrast, a double-rocker compatibility linkage will restrict the range of β_2 [17–19]. In the latter case, one can expect solutions only for a limited range of β_2, clockwise or counterclockwise—thus larger values of $\pm\beta_2$ are rare. This is a quite useful design rule.

Applying the Grashof theory to a compatibility linkage reveals some interesting behavior. Depending on the type of mechanism formed by the compatibility equations (Grashof vs non-Grashof, crank-rocker, double-rocker, etc.), solution regions may emerge. If a compatibility linkage has more than one branch (e.g., more than one unique configuration, such that reaching the second configuration requires temporarily removing at least one pin joint), then there will correspondingly be multiple sets of β_2 values that produce viable solutions. This can be seen in reference [18] (p. 4), depicting the Center-point Burmester curve for a double-rocker compatibility linkage.

A non-Grashof triple-rocker mechanism, on the other hand, has a single circuit. As a result, it will have continuous solutions throughout its full potential range of motion of the input angle. However, this will still not cover a full 360 degrees, as rockers are inherently limited in this regard.

J.A. Schaaf and J.A. Lammers furthered this research, identifying fourteen specific classes of compatibility linkages and their corresponding center-point curve shapes [19]. These fourteen groups are divided into three categories; Grashof, non-Grashof, and change-point mechanisms. Within each of these groups, depending on which link $\boldsymbol{\Delta_{1-4}}$ is the shortest, the general shape of the center-point curve can be determined. See their paper for a full list of these categories [19]. While this theory has presently only been applied to the compatibility linkage of a dyad in four precision positions, there is reason to believe that

the same line of analysis may yield similar findings for the triad in five precision positions, and perhaps even higher numbers of precision positions.

Applying the Grashof criteria to the compatibility linkage is not the same as applying the same criteria to the finished solution. Its use for the compatibility linkage reveals interesting information about potential solution regions in which, for any value of β_2, a solution exists, or regions where no dyad/triad solutions exist. However, mechanisms produced from the compatibility linkage approach may still be subject to circuit, branch, and order defects. Additionally, they may have poor force properties or low transmission angles.

2.8. Defects

The compatibility linkage is useful in that it reveals numerous prospective solutions, but the designer will still need to determine if a candidate mechanism found by this method meets their requirements and that it does not exhibit defects, such as the combination of dyads selected not reaching all design positions on one circuit of the mechanism. Chase and Mirth detailed an effective procedure for identifying and addressing these defects [29]. Whether there is a relationship between the Grashof type of compatibility linkage and any or all these properties remains a possible area for research. Similarly, applying the Grashof criteria to the higher-order compatibility linkages could be further investigated. Investigating the circuit defects of a compatibility linkage will reveal unique solution regions as there are gaps where no solutions exist for a particular value of β_2.

2.9. Eight or More Precision Positions

Cases that would require more than seven precision positions are less common in industry, as usually, a less complex solution method can produce a satisfactory mechanism design. However, a few options are available if a designer wishes to move beyond this limit. First, Chuen-Sen Lin derived compatibility linkage solutions for quadriads in up to nine positions. The solution structures produced for these mechanisms are quite complex but are solved in largely the same way as the dyads and triads. See his work from the University of Minnesota [21] or the subsequent work he and his students completed at the University of Alaska Fairbanks [30,31].

2.10. Connections to General Burmester Theory

Burmester Theory underpins many of the precision position synthesis techniques in the field of mechanisms. The theory largely revolves around the position of the poles for a particular moving plane. They are found by identifying the intersection of the perpendicular bisectors between two positions for two arbitrary points on the moving plane. In four positions, the center-point curve passes through the six standard poles, while the circle-point curve passes through the poles $\mathbf{P_{12}}$, $\mathbf{P_{13}}$, $\mathbf{P_{14}}$, and the image poles $\mathbf{P_{23}}'$, $\mathbf{P_{24}}'$ and $\mathbf{P_{34}}'$.

In addition to the poles, points called "opposite pole quadrilaterals", or "$\mathbf{\Pi}$-points", are found by identifying the intersection of lines passing through each pair of non-adjacent poles. There are twelve of these points in four positions. The first six are shown in Equation (23), each of which intersects the center-point curve, much like the natural poles.

$$
\begin{aligned}
\mathbf{\Pi_{12}} &= \overline{P_{13}P_{23}} \; x \; \overline{P_{13}P_{23}} & \mathbf{\Pi_{13}} &= \overline{P_{12}P_{23}} \; x \; \overline{P_{14}P_{34}} \\
\mathbf{\Pi_{14}} &= \overline{P_{12}P_{24}} \; x \; \overline{P_{13}P_{34}} & \mathbf{\Pi_{23}} &= \overline{P_{12}P_{13}} \; x \; \overline{P_{24}P_{34}} \\
\mathbf{\Pi_{24}} &= \overline{P_{12}P_{14}} \; x \; \overline{P_{23}P_{34}} & \mathbf{\Pi_{34}} &= \overline{P_{13}P_{14}} \; x \; \overline{P_{23}P_{24}}
\end{aligned}
\tag{23}
$$

[32,33] (pp. 25–26).

The next six are formed from some combination of the image poles and are shown in Equation (24). The circle point curve passes through each of these points in addition to the poles listed above.

$$\begin{aligned}
\Pi_{12}^1 &= \overline{P_{13}P_{23}^1} \; x \; \overline{P_{14}P_{24}^1} \quad & \Pi_{13}^1 &= \overline{P_{12}P_{23}^1} \; x \; \overline{P_{14}P_{34}^1} \\
\Pi_{14}^1 &= \overline{P_{12}P_{24}^1} \; x \; \overline{P_{13}P_{34}^1} \quad & \Pi_{23}^1 &= \overline{P_{12}P_{13}} \; x \; \overline{P_{24}^1P_{34}^1} \\
\Pi_{24}^1 &= \overline{P_{12}P_{14}} \; x \; \overline{P_{23}^1P_{34}^1} \quad & \Pi_{34}^1 &= \overline{P_{13}P_{14}} \; x \; \overline{P_{23}^1P_{24}^1}
\end{aligned} \tag{24}$$

[32,33] (pp. 25–26).

Using the full collection of these points, an initial depiction of both Burmester curves can be drawn. This visual tool may lend exceptional value. A sample plot of the Burmester curves for a dyad can be seen in Figure 15:
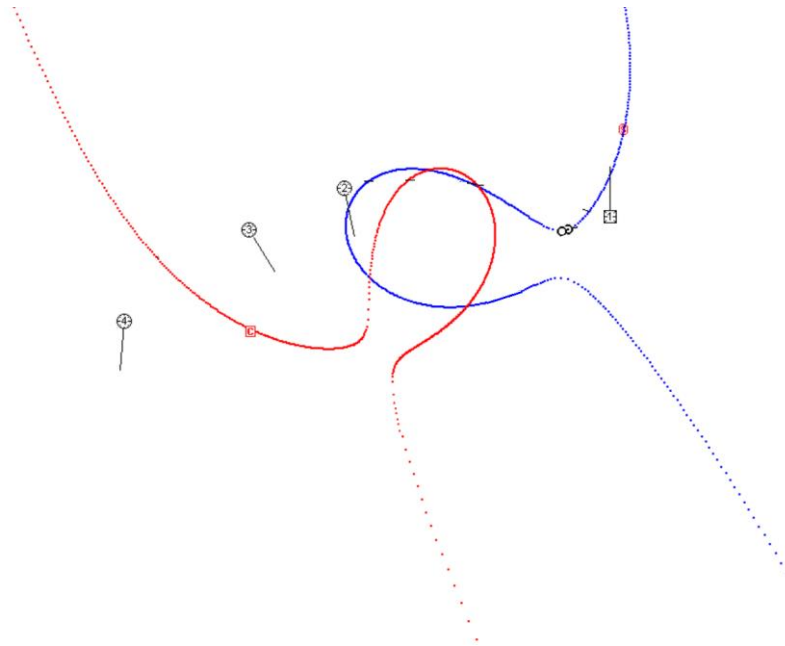
Figure 15. An example of the center-point and circle-point Burmester curves for a dyad in four positions [33].

Similarly, the Burmester Curve of Triad is shown in Figure 16:

Figure 16. The three Burmester curves for a triad in six precision positions. There are two circle-point curves (corresponding to the two moving pivots) and one center-point curve [21] (p. 86).

Each point on the Burmester curve is part of a 'Burmester Point Pair', or a Burmester point set in the case of the triad. These pairs represent a corresponding moving pivot location and ground pivot location. The method of compatibility linkages is an extremely effective tool for finding these curves—for each value of the free choice that is valid, a new pair of points in the curves is generated.

2.11. Closing Thoughts

The potential applications of kinematic synthesis through the compatibility linkage are intriguing, and there are still opportunities for further investigation. Throughout this paper β_2 has been used as the free choice, and the compatibility linkage has been applied to find the values of the angles $\beta_{i\text{-}j}$. For dyads, this paper assumes the designer wants to solve the problem for motion generation. However, by forming new cofactor matrices about α rather than β, the compatibility linkage could be used for path with prescribed timing problems as well. The LINCAGES software package utilized this realization [34–36]. Similarly for triads, it should be possible to use the compatibility linkage to solve the standard form equation for any of the angles β, α or γ, with the only procedural change being rewriting the cofactor matrices. This would allow the designer to solve triad synthesis problems defined for motion generation or for path with prescribed timing. There are typically two path generators for each motion generator due to cognates [4]. As a result, further investigation into the unique properties of the compatibility linkage and their cognates is warranted.

Schaaf and Lammers investigated the compatibility linkage of a dyad in four positions and found that its Grashof type played a distinctive role in determining the shape of the Burmester curves [19]. Inspired by their findings, we speculate that the compatibility linkage of the triad for five precision positions will exhibit similar properties. The triad has a five-bar compatibility linkage with two degrees of freedom, but it only has a single loop. Additionally, after setting the angle of one of the free choices (e.g., β_5), the rest of the linkage behaves like a four-bar, and the second free choice can be rotated through all its values (e.g., β_2). This likely means that the findings of Schaaf and Lammers are applicable to the triad, and that for each free choice of β_5 a new center-point curve could be generated which resembles the corresponding class of dyads.

In addition to the applications for multiple prescribed position synthesis, we speculate that the compatibility linkage can be utilized for mixed position-velocity synthesis as well. Using the standard form equations mixed position-velocity synthesis is already possible. In a two-precision position problem, for example, a designer may choose to include a third equation describing the velocity of the precision point in the first position. The standard form equation can be rewritten as:

$$\boldsymbol{W}\left(e^{i\dot{\beta}_j} - 1\right) + \boldsymbol{Z}\left(e^{i\dot{\alpha}_j} - 1\right) = \boldsymbol{V}_j \tag{25}$$

Here $\dot{\beta}_j$ and $\dot{\alpha}_j$ represent the angular velocities of their respective links, and $\boldsymbol{V}_j$ is the velocity vector of the precision point. To evaluate this expression using a compatibility linkage, the cofactors would need to be rewritten, but after making that change the general solution procedure should flow in exactly the same way [4,37,38].

Multiple researchers have demonstrated using multiply separated positions to synthesize a path generation mechanism by using derivative equations [4] (pp. 239–245), [39]. The resultant tracer point curve closely resembles a prescribed function for a significant range of that function. However, to achieve this result for a problem defined by a single position and its four derivatives, Sylvester's dialytic eliminant was employed. In the same way as before, we speculate that this method can be avoided by employing the compatibility linkage method. This would only require rewriting the cofactor matrices with appropriate derivatives.

3. Conclusions

In this paper, the compatibility linkage approach to kinematic synthesis has been shown to have broad applicability to a large range of linkage mechanisms. Computationally, it is a simplified way of traversing the solution space of potential dyads and triads. Similarly, the method adds the ability to visualize spatial properties of the solution space which are not easily identified through other methods. The process of using the assembled compatibility linkage to find solutions flows naturally from common mechanism analysis techniques, meaning that once completed, the compatibility linkage can be used to generate numerous potential solutions. Furthermore, while the scope of the method presented in this paper is already quite unifying, there remain many opportunities to expand the method even further through additional research.

Appendix A. Detailed Solution Procedure for a Triad in Six and Seven Precision Positions Using the Method of Compatibility Linkages

Triad in six precision positions:
Displacement equations:

$$\begin{bmatrix} e^{i\alpha_2}-1 & e^{i\beta_2}-1 & e^{i\gamma_2}-1 & \delta_2-h_2 \\ e^{i\alpha_3}-1 & e^{i\beta_3}-1 & e^{i\gamma_3}-1 & \delta_3-h_3 \\ e^{i\alpha_4}-1 & e^{i\beta_4}-1 & e^{i\gamma_4}-1 & \delta_4-h_4 \\ e^{i\alpha_5}-1 & e^{i\beta_5}-1 & e^{i\gamma_5}-1 & \delta_5-h_5 \\ e^{i\alpha_6}-1 & e^{i\beta_6}-1 & e^{i\gamma_6}-1 & \delta_6-h_6 \end{bmatrix} \begin{bmatrix} \vec{W} \\ \vec{V} \\ \vec{Z} \\ -1 \end{bmatrix} = \vec{0} \tag{A1}$$

[21] (p. 22).

As with a dyad in five positions, there are two compatibility equations to solve simultaneously from this matrix. They are:

$$\Delta_2 e^{i\beta_2} + \Delta_3 e^{i\beta_3} + \Delta_4 e^{i\beta_4} + \Delta_5 e^{i\beta_5} + \Delta_1 = 0 \tag{A2}$$

And:

$$\Delta'_2 e^{i\beta_2} + \Delta'_3 e^{i\beta_3} + \Delta'_4 e^{i\beta_4} + \Delta_5 e^{i\beta_6} + \Delta'_1 = 0 \tag{A3}$$

[21] (p. 23).

Once the Δ terms have been defined, the compatibility linkage is drawn. As before, align the tails of vectors Δ_2 and Δ_2', and rotate the Δ' loop (keeping inter-link angular relations constant) so that Δ_2 and Δ_2' point in the same direction. In this case, there are two parallelogram loops to form. The first is the loop BCEF, and the second is GIJK, as seen below.

Note that Figure A1 was generated slightly differently from the previous compatibility linkages. Here, Δ_3 and Δ_3' were chosen as the ground pivots, and these links were overlaid with each other, with the head rather than the tail of Δ_2 taken as the common point between the two loops. As a result, the parallelogram BCEF is formed about the link Δ_4 and Δ_4' (Δ_4 is extended to form the ternary link CDE), while the parallelogram GIJK was formed about

links Δ_1 and Δ_1' (Δ_1 is extended to form the ternary link HIJ). Finally, a ternary link AJK is formed incorporating Δ_2 and Δ_2' (connecting the points J and K). A critical observation to make regarding these parallelogram loops is that each was made possible by existing relationships between the Δ and Δ' terms. Δ_2 and Δ_2' share the same angular displacement, even prior to being connected. The same is true of Δ_3 and Δ_3', and Δ_4 and Δ_4'. This means that combining these links is an unnecessary but helpful simplification of the compatibility linkage, as this new form above requires only a single input to fully determine the rest of the mechanism. This is a significant advantage, as each independent five-bar loop had two degrees of freedom, making the problem more complex.
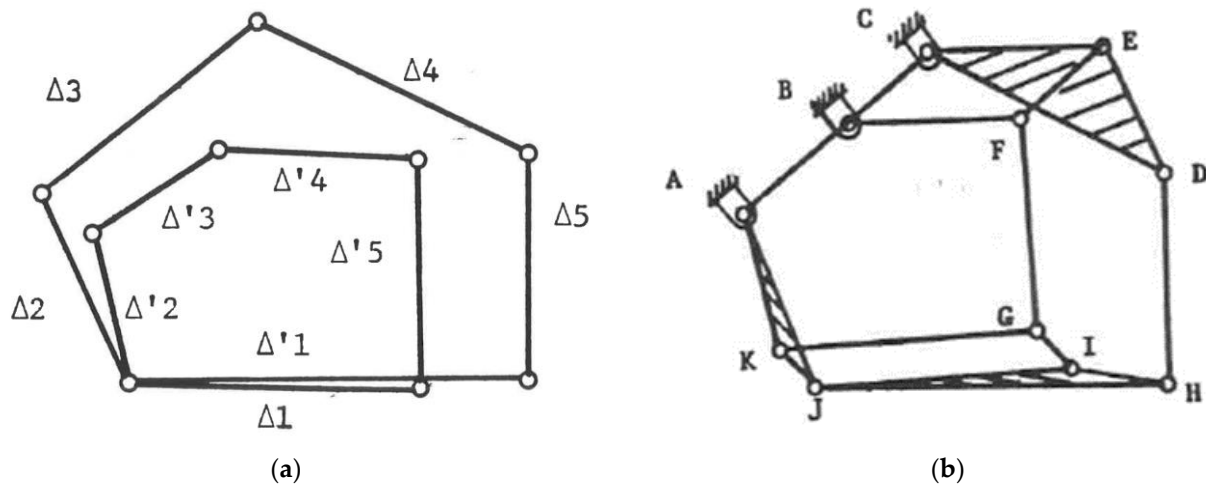
Figure A1. (**a**) The two loops of the triad in six positions shown without modification; (**b**) The compatibility linkage of a triad in six positions after aligning Δ_3 and forming parallelograms [21] (pp. 31–35).

The compatibility linkage of the triad in six positions can be used to find solutions in the form described above. However, the linkage is unique in that it has an additional layer of possible simplification that the designer can take advantage of. As was discussed earlier, the number of unique geometric inversions of the compatibility linkage corresponds to the number of unique solutions to the original problem. In this case, though, once the free-choice angle β_2 is selected and implemented, the relative positions of links AJK and HIJ remain consistent regardless of which geometric inversion is considered. As a result, several links can be eliminated. The pivots A, G, and H can be considered as a single ternary link, reducing the ten-bar linkage to a seven-bar zero-DOF structure [17] (p. 36). After implementing each of these steps, the new structure looks like this (Figure A2):
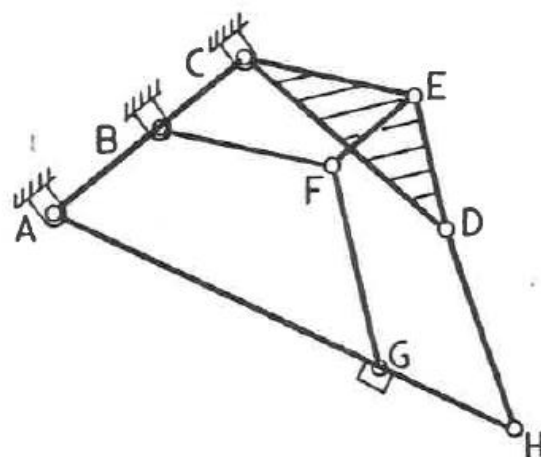

Figure A2. The simplified form of the compatibility linkage for a triad in six positions [21] (p. 38).

The final positions of each of the points in this compatibility linkage are shown in Table A1. To find solutions, remove the link EF, creating a Watt-II solution linkage. For positions (apart from the starting position) in which links, CE and BF are parallel, the mechanism represents a solution to the original problem.

Table A1. Simplified compatibility linkage global point positions (triad, 6PP).

Point	Position in Plane
A	$(0,0)$
B	Δ_3'
C	Δ_3
D	$\Delta_3 + \Delta_4$
E	$\Delta_3 + \Delta_4'$
F	$\Delta_3' + \Delta_4'$
G	$-\Delta_2' + \Delta_1$
H	$-\Delta_2 + \Delta_1$

The solution values are then taken from the angular displacements of links AH, BF, HD, and GF, which correspond to the values of $-\beta_3$, $\beta_4-\beta_3$, $\beta_5-\beta_3$, and $\beta_6-\beta_3$, respectively. These relationships are shown in Table A2. While making these simplifications does take more time initially, the payoff is substantial. Analysis of a six-bar mechanism is easier than a ten-bar linkage, not to mention that the Watt-type mechanisms are much more thoroughly covered in the literature. A designer working through this process will find the following relations:

Table A2. Selected Links in the simplified compatibility linkage and their corresponding beta values.

Link	Angular Displacement
AH	$-\beta_3$
BF *	$\beta_4-\beta_3$
HD	$\beta_5-\beta_3$
GF	$\beta_6-\beta_3$

* BF or CE can be used, as they share the same angular displacement.

The attentive reader may note that the angle β_2 is neglected in Tables A1 and A2, and it no longer plays a role as a free choice or as a solution angular displacement. Fortunately, once the beta values have been calculated, not all of them must be used. Only three of the beta values need to be incorporated to calculate the value of each unique solution for the triad. Chuen-Sen Lin shows an example, here taken as Equation (A4), using β_2, β_3, and β_4.

$$\begin{bmatrix} \vec{W} \\ \vec{V} \\ \vec{Z} \end{bmatrix} = \begin{bmatrix} e^{i\alpha_2} - 1 & e^{i\beta_2} - 1 & e^{i\gamma_2} - 1 \\ e^{i\alpha_3} - 1 & e^{i\beta_3} - 1 & e^{i\gamma_3} - 1 \\ e^{i\alpha_4} - 1 & e^{i\beta_4} - 1 & e^{i\gamma_4} - 1 \end{bmatrix}^{-1} \begin{bmatrix} \delta_2 - h_2 \\ \delta_3 - h_3 \\ \delta_4 - h_4 \end{bmatrix} \tag{A4}$$

[21] (p. 39).

The solutions to this reduced system of standard form equations are the final solutions to the precision position problem.

Triad in seven precision positions:

A triad in seven precision positions is by far the most mathematically complex of the compatibility linkage types listed here. As with the transition from four to five positions for a dyad, the transition from six to seven positions for a triad reduces the number of potential solutions from an infinite number (based on the infinite number of potential free choice values) to a finite value, Solutions come in sets of 0, 2, 4, or 6 depending on the intersections of the Burmester curves. As a result, most authors recommend refraining

from using seven positions when synthesizing triads. The benefits of having a free choice almost always outweigh the cost of giving up a precision position. With that said, should a designer choose to proceed with the compatibility linkage approach to a triad in seven positions, they'll find that there are three compatibility equations that must be fulfilled. These equations are shown below, with loop one:

$$\Delta_2 e^{i\beta_2} + \Delta_3 e^{i\beta_3} + \Delta_4 e^{i\beta_4} + \Delta_5 e^{i\beta_5} + \Delta_1 = 0 \tag{A5}$$

Loop Two:

$$\Delta'_2 e^{i\beta_2} + \Delta'_3 e^{i\beta_3} + \Delta'_4 e^{i\beta_4} + \Delta_5 e^{i\beta_6} + \Delta'_1 = 0 \tag{A6}$$

Loop Three:

$$\Delta''_2 e^{i\beta_2} + \Delta''_3 e^{i\beta_3} + \Delta''_4 e^{i\beta_4} + \Delta_5 e^{i\beta_7} + \Delta''_1 = 0 \tag{A7}$$

[21] (p. 115).
where,

$$\Delta_1 = -\Delta_2 - \Delta_3 - \Delta_4 - \Delta_5 \tag{A8}$$

$$\Delta'_1 = -\Delta'_2 - \Delta'_3 - \Delta'_4 - \Delta_5 \tag{A9}$$

$$\Delta''_1 = -\Delta''_2 - \Delta''_3 - \Delta''_4 - \Delta_5 \tag{A10}$$

Conveniently, as with the previous analyses of triads, each of these compatibility equations represents a five-bar chain in the compatibility linkage. As a result, the setup of the linkage, in this case, will feel quite familiar. As before, the angular displacements of some equivalent Δ terms are equal. Now, however, a third link is added to each set, yielding $(\Delta_2, \Delta_2', \Delta_2'')$, $(\Delta_3, \Delta_3', \Delta_3'')$, and $(\Delta_4, \Delta_4', \Delta_4'')$. In response to some stimulus in the mechanism, each of these links in the compatibility linkage will have the same displacement angle as the others in its set. This allows for the forming of several sets of parallelograms between the different chains formed from the compatibility equations. The chains start out in the form shown in Figure A3.
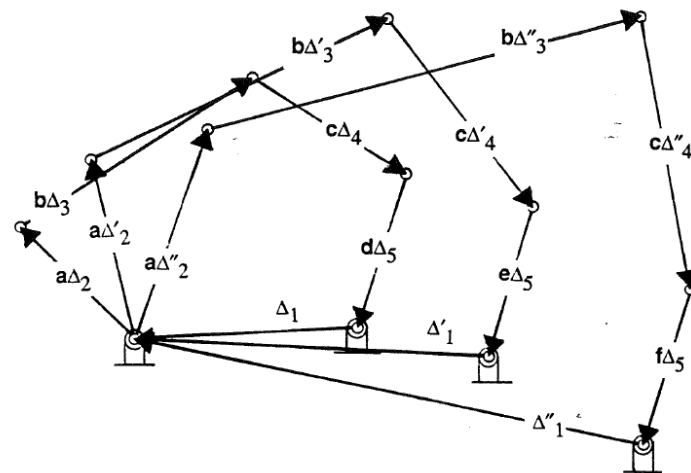

Figure A3. The three loops of the triad compatibility linkage for seven precision positions prior to modification. The end of link Δ_1 is selected as the common point [21] (p. 116).

After rotating the links to create alignment and creating the appropriate parallelograms between each layer of the loop, the linkage takes the form shown in Table 2. Links IJ, IH, MP, and PQ have all been created to form parallelogram loops. These parallel motion structures are created around links Δ_1, Δ_2, Δ_3, and Δ_4, which were each of the links that had identical angular displacement relationships. As with the lower-order structures, the designer may use this linkage by removing any of these created links, changing the chain from a 15-bar zero-degree-of-freedom structure to a 14-bar one-degree-of-freedom linkage. From here, the

designer must identify the mechanism positions (outside of the starting position) in which the sides of the parallelogram from which the link was removed are parallel to each other. At these positions, the angular displacements of links CD, DE, EH, HM, KN, and LO from their starting positions correspond to β_2-β_7, respectively [21] (p. 115). Further simplifications of the compatibility linkage for a triad in seven precision positions remain an area for further study.

Appendix B. Special Cases of the Triad Compatibility Linkage

Figure A4. Special cases of the triad compatibility linkage [21] (p. 50).

References

1. Needham, J. *Science and Civilisation in China—Volume 4: Physics and Physical Technology*; Cambridge University Press: Cambridge, UK, 1971. Available online: https://archive.org/details/principlesmecha02willgoog (accessed on 7 November 2022).
2. Compass. Available online: https://education.nationalgeographic.org/resource/compass (accessed on 7 November 2022).
3. Willis, R. *Principles of Mechanism*; Nabu Press: Charleston, SC, USA, 2010. Available online: https://archive.org/details/principlesmecha02willgoog/page/n8/mode/2up (accessed on 7 November 2022).
4. Sandor, G.N.; Erdman, A.G. *Advanced Mechanism Design: Analysis and Synthesis*; Pearson: New York, NY, USA, 1984; Volume 2, ISBN 978-0130114372.
5. Wampler, C.W.; Morgan, A.P.; Sommese, A.J. Numerical Continuation Methods for Solving Polynomial Systems Arising in Kinematics. *J. Mech. Des.* **1990**, *112*, 59–68. [CrossRef]
6. Subbian, T.; Flugrad, D.R. Four-Bar Path Generation Synthesis by a Continuation Method. *J. Mech. Des.* **1991**, *113*, 63–69. [CrossRef]
7. Subbian, T.; Flugrad, D.R. Six and Seven Position Triad Synthesis Using Continuation Methods. *J. Mech. Des.* **1994**, *116*, 660–665. [CrossRef]
8. Pathak, V.K.; Singh, R.; Sharma, A.; Kumar, R.; Chakraborty, D. A Historical Review on the Computational Techniques for Mechanism Synthesis: Developments Up to 2022. *Arch. Comput. Methods Eng.* **2022**. [CrossRef]
9. Deshpande, S.; Purwar, A. Computational creativity via assisted variational synthesis of mechanisms using deep generative models. *J. Mech. Des. Trans. ASME* **2019**, *141*, 121402. [CrossRef]
10. Baskar, A.; Bandyopadhyay, S. An algorithm to compute the finite roots of large systems of polynomial equations arising in kinematic synthesis. *Mech. Mach. Theory* **2019**, *133*, 493–513. [CrossRef]
11. Zhao, P.; Ge, X.; Zi, B.; Ge, Q.J. Planar linkage synthesis for mixed exact and approximated motion realization via kinematic mapping. *J. Mech. Robot.* **2016**, *8*, 051004. [CrossRef]
12. Re, F.M.; Williams, J.O. Chaise Lounge Recliner Chair. U.S. Patent 5,090,768A, 17 July 1991.
13. Chase, T.R.; Erdman, A.G.; Riley, D.R. Triad Synthesis for up to Five Design Positions With Application to the Design of Arbitrary Planar Mechanisms. *J. Mech. Transm. Autom. Des.* **1987**, *109*, 426–434. [CrossRef]
14. Freudenstein, F.; Sandor, G.N. Synthesis of Path-Generating Mechanisms by Means of a Programmed Digital Computer. *J. Eng. Ind.* **1959**, *81*, 159–167. [CrossRef]
15. Hartenberg, R.; Denavit, J. *Kinematic Synthesis of Linkages*; McGraw-Hill: New York, NY, USA, 1964. Available online: https://idoc.pub/documents/r-hartenberg-j-denavit-kinematic-synthesis-of-linkages-1964pdf-jlk92zy1r745 (accessed on 10 November 2022).
16. Hayes, M.J.D.; Zsombor-Murray, P.J. Solving the Burmester Problem Using Kinematic Mapping. In Proceedings of the ASME 2002 International Design Engineering Technical Conferences and Computers and Information in Engineering Conference. Volume 5: 27th Biennial Mechanisms and Robotics Conference, Montreal, QC, Canada, 29 September–2 October 2002; pp. 1439–1446. [CrossRef]
17. Myszka, D.H.; Murray, A.P. Identifying sets of four and five positions that generate distinctive center-point curves. In Proceedings of the ASME 2009 International Design Engineering Technical Conferences and Computers and Information in Engineering Conference, San Diego, CA, USA, 30 August–2 September 2009; pp. 463–473. [CrossRef]
18. Chase, T.R.; Erdman, A.G.; Riley, D.R. Improved Centerpoint Curve Generation Techniques for Four-Precision Position Synthesis Using the Complex Number Approach. *J. Mech. Trans. Autom.* **1985**, *107*, 370–376. [CrossRef]
19. Schaaf, J.A.; Lammers, J.A. Geometric Characteristics of the Center-Point Curve Based on the Kinematics of the Compatibility Linkage. In Proceedings of the ASME 1992 Design Technical Conferences. 22nd Biennial Mechanisms Conference: Mechanism Design and Synthesis, Scottsdale, AZ, USA, 13–16 September 1992; pp. 475–480. [CrossRef]
20. Sakurai, S. Three-Position Variable Camber Krueger Leading Edge Flap. U.S. Patent 5,158,252A, 24 October 1991.
21. Lin, C.S. Dimensional Synthesis of a Planar Triad for Six Precision Positions. Ph.D. Thesis, University of Minnesota, Twin Cities, MN, USA, 1987.
22. Erdman, A.G.; Lonn, D. A Unified Synthesis of Planar Six-Bar Mechanisms Using Burmester Theory. In Proceedings of the Fourth World Congress on the Theory of Machines and Mechanisms, Newcastle Upon Tyne, UK, 8–12 September 1975; pp. 867–872.
23. Berneman, C.; Bican, L.; Howard, M.; Oladepo, I. Kinematic Synthesis of a Drone Tilt Mechanism. *Univ. Minn. Twin Cities Adv. Mech. Des.* **2022**, *1*, 1–29.
24. Rector, D.M. Linkage Mechanism Designer and Simulator. 2019. Available online: www.linkagesimulator.com (accessed on 6 September 2022).
25. Rank of a Matrix. Available online: https://www.cuemath.com/algebra/rank-of-a-matrix/ (accessed on 17 October 2022).
26. Erdman, A.G.; Chase, T.R. New Software Synthesizes Complex Mechanisms. *Mach. Des.* **1985**, *57*, 107–113.
27. Erdman, A.G.; Chase, T.R. New software synthesizes complex mechanisms. *Mach. Des.* **1985**, *57*, 107–109.
28. Yu, N.; Erdman, A.G.; Byers, B.P. LINCAGES 2000: Latest Developments and Case Study. In Proceedings of the ASME 2002 International Design Engineering Technical Conferences and Computers and Information in Engineering Conference. Volume 5: 27th Biennial Mechanisms and Robotics Conference, Montreal, QC, Canada, 29 September–2 October 2002; pp. 1421–1425. [CrossRef]
29. Mirth, J.A.; Chase, T.R. Circuit Rectification for Four Precision Position Synthesis of Four-Bar and Watt Six-Bar Linkages. *J. Mech. Des.* **1995**, *117*, 612–619. [CrossRef]

30. Lin, C.-S.; Erdman, A.G.; Jia, B.-P. Use of Compatibility Linkages and Solution Structures in the Dimensional Synthesis of Mechanism Components. *Mech. Mach. Theory* **1996**, *31*, 619–635. [CrossRef]
31. Lu, X. A New Method to Group the Solutions from Dimensional Synthesis of Planar Triads for Six Prescribed Precision Positions. Master's Thesis, University of Alaska, Fairbanks, AK, USA, 1992; p. 118.
32. Mlinar, J.R.; Erdman, A.G. An Introduction to Burmester Field Theory. *J. Mech. Des.* **2000**, *122*, 25–30. [CrossRef]
33. Mlinar, J.R. An Examination of the Features of the Burmester Field and the Linear Solution Geometry of Dyads and Triads. Ph.D. Thesis, University of Minnesota, Twin Cities, MN, USA, 1997.
34. Peterson, R.; Logan, L.; Erdman, A.G.; Riley, D.R. Three Precision Point Synthesis of a Four Bar Linkage: An Example Using the LINCAGES-4 Program. In Proceedings of the Computers in Engineering 1988 Conference, San Francisco, CA, USA, 31 July–4 August 1988; pp. 91–96.
35. Erdman, A.G.; Gustafson, J.E. LINCAGES: Linkage Interactive Computer Analysis and Graphically Enhanced Synthesis Package. *Am. Soc. Mech. Eng. (Pap.)* **1977**, *77*, 77-DET-5.
36. Nelson, L.; Erdman, A.G. Recent Enhancements to the LINCAGES-6 Synthesis Package, including Circuit Rectification. In Proceedings of the ASME 1994 Design Technical Conferences collocated with the ASME 1994 International Computers in Engineering Conference and Exhibition and the ASME 1994 8th Annual Database Symposium. 23rd Biennial Mechanisms Conference: Mechanism Synthesis and Analysis, Minneapolis, MN, USA, 11–14 September 1994; pp. 263–271. [CrossRef]
37. Holte, J.E.; Chase, T.R.; Erdman, A.G. Approximate Velocities in Mixed Exact-Approximate Position Synthesis of Planar Mechanisms. *J. Mech. Des.* **1999**, *123*, 388–394. [CrossRef]
38. Holte, J.E.; Chase, T.R.; Erdman, A.G. Mixed Exact-Approximate Position Synthesis of Planar. *J. Mech. Des.* **2000**, *122*, 278–286. [CrossRef]
39. Tesar, D.; Sparks, J.W. Multiply Separated Position Synthesis. *ASME Paper* **1968**, *3*, 68-MECH-66. [CrossRef]